Environment Canada

Water Science and Technology Directorate

Direction générale des sciences et de la technologie, eau

Environnement Canada

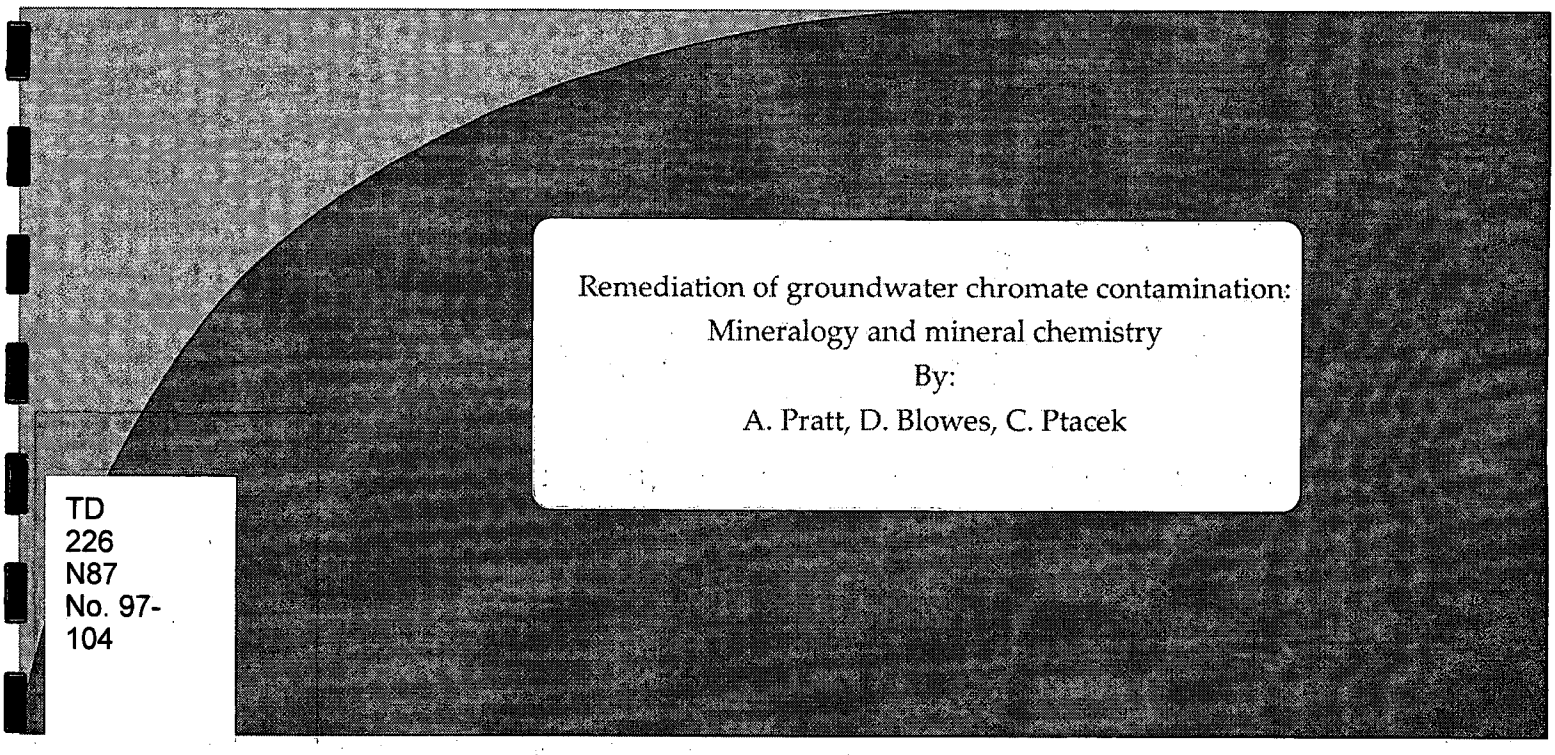

Remediation of groundwater chromate contamination: Mineralogy and mineral chemistry

By:

A. Pratt, D. Blowes, C. Ptacek

97-104

MANAGEMENT PERSPECTIVE

Title: Remediation of groundwater chromate contamination: mineralogy and mineral chemistry.

Author: A.R. Pratt, D.W. Blowes, and **C.J. Ptacek**

NWRI Publication#: 97-104

Citation: Environmental Science and Technology

EC Priority/Issue: This work supports the ESD Issue "Conserving Canada's Ecosystems" (metals) and the business plan deliverables Thrust #3 (groundwater remediation). It also supports the EC Action Plan "Conserving Canada's Ecosystems" with the focus "Develop and implement strategies to conserve ecosystems". The study was initiated in 1991 and was funded by the University of Waterloo and Surface Science Western.

Current Status: The paper describes the mineralogy and mineral chemistry of long-term column studies conducted to assess the potential for in-situ treatment of chromate contaminated groundwater using permeable reactive walls. Chromium in the form of chromate is one of the most frequently encountered contaminants in groundwater. In the hexavalent form, Cr is highly toxic and carcinogenic. The study was initiated in 1992. Mineralogical analyses of reacted solids after flowing Cr(VI) contaminated groundwater through treatment materials for several years are presented.

Next Steps: In-situ remediation appears to be a viable technique for remediation of a number of inorganic contaminants. Future efforts will be directed toward the development of techniques for remediating a variety of inorganic contaminants.

Abstract

Groundwater containing aqueous Cr(VI) species are an environmental concern worldwide. Cr(VI) removal using permeable-reactive redox walls constructed using iron filings have been recently shown as an effective remediation method. Iron filings reacted with Cr(VI) doped solutions in flow-through column studies are found to develop oxidized coatings comprised of goethite. Mineralogical analysis shows chromium to be concentrated in the outermost edge of the coatings. Surface analysis identifies all detectable chromium occurs exclusively as Cr(III) species. In addition it is found that with increased chromium content goethite surfaces acquire chemical and structural characteristics similar to Fe_2O_3. Accumulation of discrete Cr_2O_3 globules is observed, suggesting a complete partitioning of chromium from the surface iron oxide species. Results of the study indicate complete reduction of Cr(VI) to Cr(III) occurs and that Cr(III) is incorporated into solid species which are sparingly soluble.

Products of Chromate Reduction on Proposed Subsurface Remediation Material

ALLEN R. PRATT,*,† DAVID W. BLOWES,† AND CAROL J. PTACEK‡

Department of Earth Sciences, University of Waterloo, Waterloo, Ontario, Canada, N2L 3G1, and National Water Research Institute, Environment Canada, 867 Lakeshore Road, Burlington, Ontario, Canada L7R 4A6

Recent studies have shown promising results for subsurface remediation of dissolved chromate using permeable-reactive redox walls. Chromate reduction in the presence of iron filings and quartz grains was studied to determine the fate of reduced chromium in proposed wall material. Using a flow-through column apparatus, iron filings mixed with quartz grains were reacted with solutions that contained about 20 mg/L dissolved Cr(VI). Reacted iron filings developed coatings comprised of goethite with chromium concentrated in the outermost edges. Surface analysis showed all detectable chromium occurred as Cr(III) species. In addition, in regions of increased chromium concentration, goethite acquired chemical and structural characteristics similar to Fe_2O_3 and Cr_2O_3. Results of the study show that complete reduction of Cr(VI) to Cr(III) occurred and that Cr(III) was incorporated into sparingly soluble solid species.

Introduction

Chromium is a common groundwater contaminant in industrial regions throughout the world. In the United States chromium is the second most common inorganic groundwater contaminant, after lead (*1*). In groundwater environments, chromium occurs in two stable oxidation states, Cr(VI) and Cr(III) (*2*, *3*). Many Cr(VI) species are known carcinogens and are of environmental concern. In contrast, Cr(III) species are generally regarded as benign (*1*). Conventional groundwater treatment programs involve the pumping of contaminated groundwater for treatment and disposal of contaminants. This approach can be ineffective (*4*). A new technology currently being developed for the remediation of contaminated groundwater involves placing permeable-reactive redox walls below the ground surface in the path of flowing groundwater (*3*, *5*, *6*). Laboratory studies by Blowes and Ptacek (*5*) have shown that iron-bearing solids rapidly remove chromate from solution and may potentially be an effective redox wall material for use in subsurface chromate remediation.

Blowes et al. (*6*) conducted a series of batch and long-term dynamic flow-through column experiments designed to investigate the Cr(VI) removal potential for various iron-bearing solids. Of the materials tested, iron filings mixed with quartz sand at a 1:1 mass ratio were found to have the highest chromate removal potential. The purpose of this research is to identify the mineralogical and geochemical nature of the secondary reaction products formed on iron filings throughout the dynamic flow column tests described by Blowes et al. (*6*). The objectives of this research were accomplished by combining traditional mineralogical analysis methods with surface analysis methods.

Materials and Methods

The iron filings examined in this study were reacted with solutions containing about 20 mg/L Cr(VI), as K_2CrO_7, under dynamic flow conditions of 10 m/a for more than 150 pore volumes. Experimental methods for the column tests are reported in Blowes and Ptacek (*5*) and Blowes et al. (*6*). The grains examined here were flushed with a chromium-free calcium carbonate-saturated solution following the breakthrough of Cr(VI) in the column effluent solution (*6*). Specimens allotted for surface analysis were handled under argon or nitrogen gas atmospheres to minimize the contamination of surfaces by atmospheric gases.

Iron filing and quartz grain surfaces were analyzed using reflected light microscopy, secondary electron microscopy (SEM), energy-dispersive X-ray analysis (EDX), electron probe microanalysis (EPMA), X-ray photoelectron spectroscopy (XPS), Raman spectroscopy, and Auger electron spectroscopy (AES). XPS provides chemical state information, Raman spectroscopy structural information, and AES compositional information. Comprehensive introductions to these surface methods of analysis with regard to geologic materials are presented in Hochella (*7*) (XPS and AES) and Johnston (*8*) (Raman spectroscopy).

SEM, EDX, and EPMA. Secondary electron images were acquired using a Hitachi S-4500 field emission secondary electron microscope. Images were collected with a beam potential of 5 kV. EDX analysis were acquired using a Noran Instruments light element EDX detector attached to an ISI DS-130 scanning electron microscope. EDX spectra and X-ray maps were collected using a beam potential of 15 kV. EPMA analysis were conducted using a Jeol JXA-8600 wavelength dispersion system. The accelerating voltage was 15 kV, with a beam size near 1 μm and current of 10 nA. Analysis were calibrated for Fe and Cr using hematite and chromite reference standards.

XPS. XPS measurements were made using a modified SSX-100 X-ray photoelectron spectrometer, with a monochromatized Al Kα X-ray source (spot size 300–600 μm) and a base pressure of 2×10^{-9} Torr. The spectrometer was calibrated to the Au($4f_{7/2}$) line at 83.98 eV and gave an energy difference of 857.1 eV between the metallic copper $3p_{3/2}$ and $2p_{3/2}$ lines. Analyzer pass energies were 160 and 25 eV. Quantitative XPS measurements using integrated photoelectron line intensities were corrected using calculated photoelectron cross-sections. Metal 3p line intensities were used for quantitative measurements because of their less complex spectral backgrounds. Charge shifting of spectra was minimal, <0.6 eV, based on the position of the C(1s) hydrocarbon line at 285.0 eV.

Raman Spectroscopy. Raman spectra were recorded on a Dilor Omars 89 spectrometer using a Coherent Radiation Innova 70 argon ion laser and 514.5 nm radiation. A neon lamp was used to calibrate the spectrometer. Laser beam diameter was 5–8 μm.

AES. AES measurements were made using a Perkin Elmer Phi-600 scanning Auger microprobe. Instrument base pressure was 3×10^{-9} Torr. Surfaces were found to be susceptible to damage from the impinging electron beam. Surface damage was substantially reduced and possibly eliminated

* Corresponding author present address: Surface Science Western, The University of Western Ontario, London, Ontario, Canada N6A 5B7; fax: (519)661-3709; e-mail: apratt@surf.ssw.uwo.ca.
† University of Waterloo.
‡ Environment Canada.

S0013-936X(96)00789-4 CCC: $14.00

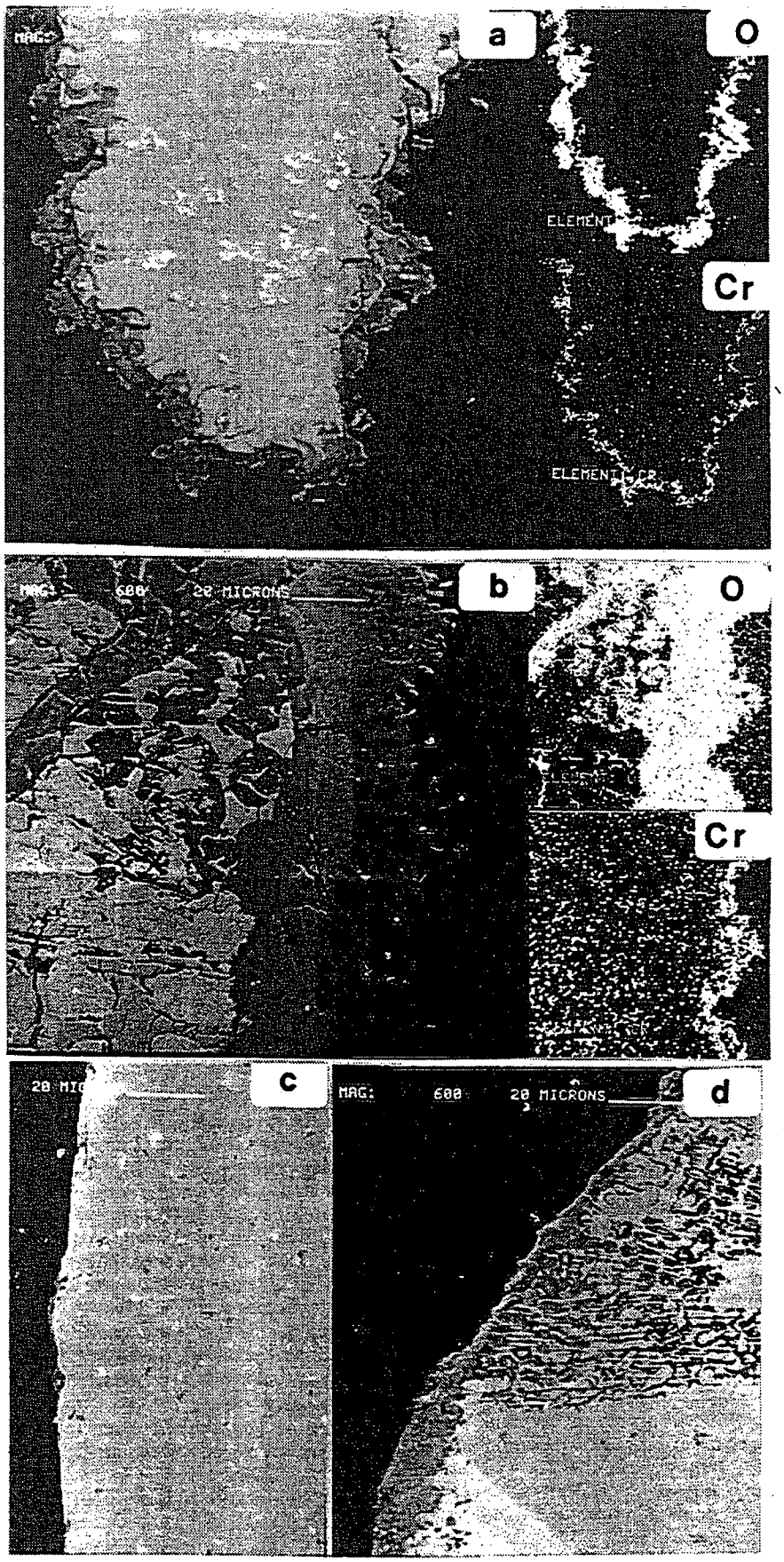

FIGURE 1. SEM micrographs and elemental X-ray maps for O and Cr illustrating the character of secondary coatings found on chromate reacted iron filings: (a) massive type coating; (b) colleform textured coating (circles and line mark EPMA and AES microprobe traverses; analysis point 1 (Table 1) is denoted by the outermost circle (three subsequent analyses points follow in sequence the series of circles inward across the coating)); (c) cross-section of unreacted iron filing; (d) cross-section showing oxidized coating present on some iron filings prior to reaction.

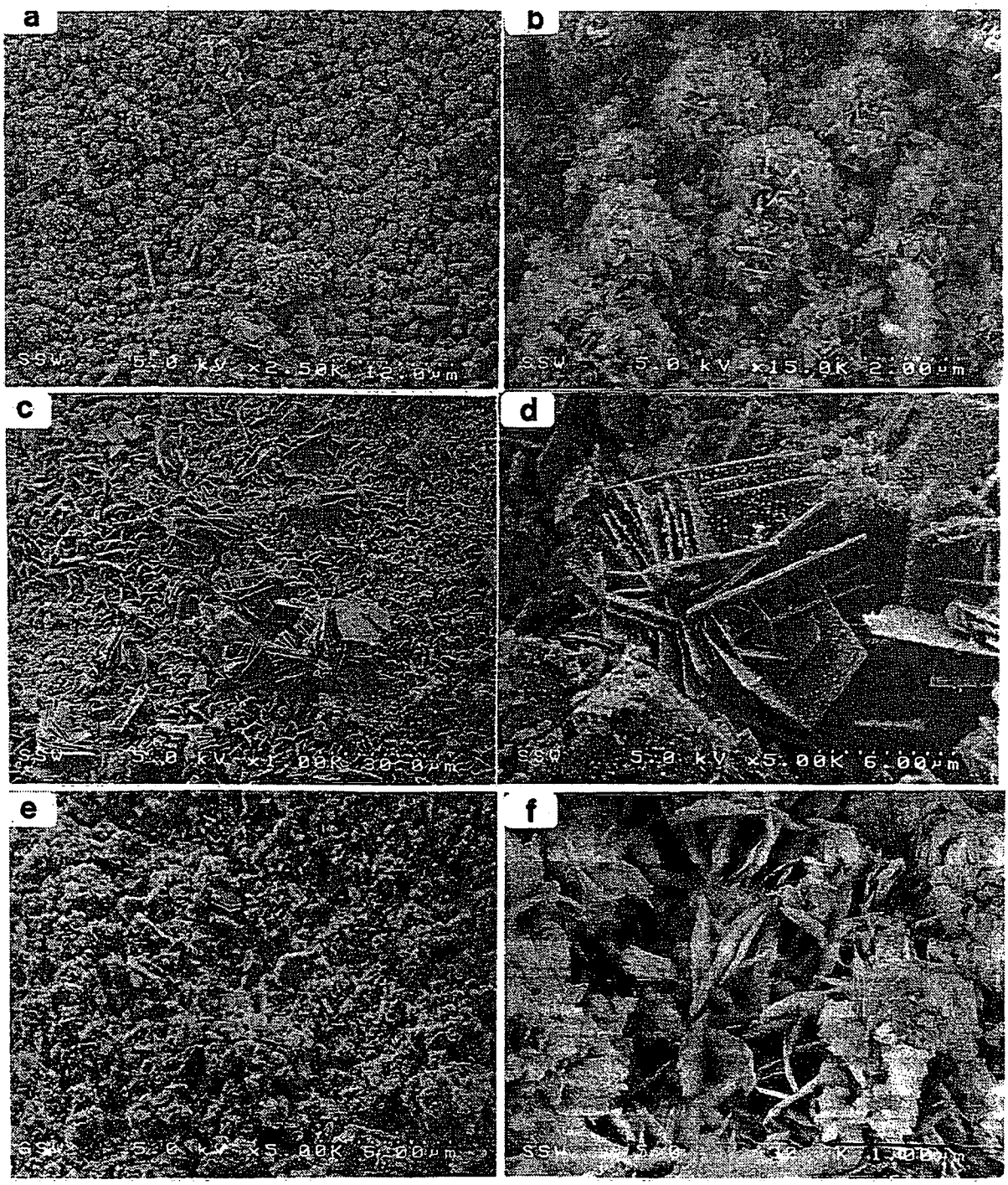

FIGURE 2. Representative SEM micrographs of oxidized coatings on reacted iron filing and quartz grains: (a and b) micrographs of botryoidal surfaces on iron filing coatings; (c and d) micrographs of euhedral plates on iron filing coatings; (e and f) micrographs of oxidized coatings on quartz grains.

using a 3 kV electron beam with a current of 3–10 nA and a beam diameter of 2–5 μm. Quantitative AES measurements using differentiated Auger line peak to peak intensities were corrected using the sensitivity factors provided by Nesbitt and Pratt (*9*) for Fe and O. Additional element intensities were corrected using manufacturer-supplied sensitivity factors.

Results and Discussion

Mineralogy of Secondary Phases. The iron filings examined are irregularly shaped and approximately 1 mm in size. The iron filings are encrusted with coatings of varying thickness with the majority in the 25–50 μm range. Replacement type textures commonly are observed along the filing grain edges. Coatings are primarily massive (Figure 1a). A small population of the grains exhibit well-defined colloform banding. Along many grain surfaces radiating crystals with an acicular habit are discernible (Figure 1b). Coatings on the iron filings and quartz grains are identified as goethite (αFeOOH), using reflected light microscopy and X-ray diffraction methods. Goethite coatings on quartz grains are thin (<25 μm) and compact.

Elemental X-ray maps for oxygen provide clear definition of the boundaries between the iron filing substrate and goethite coating (Figures 1a and 2a). Examination of chromium X-ray maps show that the highest concentrations of

TABLE 1. Measured Atomic Percent Concentrations for Fe, Cr, and O Acquired during EPMA and AES Traverse across Region of Colloform Banding Found on Reacted Iron Filing[a]

	Fe	Cr	O
Pt 1			
EPMA	21.3	1.4	76.9
AES	28.3	12.4	59.3
Pt 2			
EPMA	29.4	0.2	68.9
AES	32.8	0.0	67.2
Pt 3			
EPMA	35.9	0.1	63.0
AES	34.5	0.0	65.5
Pt 4			
EPMA	36.9	0.1	61.8
AES	33.9	0.0	66.1

[a] Analysis locations are shown in Figure 1b.

chromium are found at the outermost edges of the coatings (Figures 1a and 2a). Within these regions chromium is found to have a highly heterogeneous distribution. For example, at any randomly selected point an EDX spectra may exhibit an intense Cr-Kα line. Moving the point of analysis a few micrometers, the intensity of the Cr-Kα line can decrease to near background levels.

The formation of colloform textures on some of the grains indicates at least two periods of coating formation, which is unexpected under continuous flow conditions. The micrograph in Figure 1c shows a typical cross-section of an unreacted iron filing. This filing is largely pristine at the micrometer scale. There is however, as shown in Figure 1d, a small population of the grains (<5%) that is significantly oxidized prior to reaction. EDX spectra show the darker gray area to be comprised mainly of Fe and O. The most pronounced oxidized deposits are found on filings that contain impurities, such as P, or physical defects. These observations indicate inner colloform bands formed prior to contact with chromate-containing solutions.

Secondary electron and backscatter electron images of the colloform bands are all similar to Figure 1a,b and show distinct differences in the gray levels and sharp boundaries between bands. Differences in gray levels are generally attributed to changes in average atomic number. The increased chromium content of the outer edge does not appear to be a factor in gray level differences. Grey levels tend to be fairly consistent within regions of high chromium content whereas the distribution of chromium is extremely irregular. An EPMA traverse across the two bands shows a trend of progressive iron enrichment inward (Table 1). If the gray level differences are due to a progressive enrichment in iron, then a corresponding sequential gray level lightening across the coating should occur. The well-defined boundary between the two colloform bands demonstrates that this is not the case. The increase in iron as the filing–coating interface is approached is most likely due to progressively greater contributions to the EPMA volume of analysis from the filing substrate.

To test this hypothesis and by following the example of Hochella et al. (*10*), a traverse immediately adjacent to the EPMA points using the AES instrument as a microprobe was undertaken. AES is a microbeam surface analytical method, and any contributions from depth should be eliminated (*10*). The results of the AES transverse show that iron content remains relatively constant across the coating (Table 1). The similarity of AES analyses across the colloform bands indicates that gray level change is not due to chemical variations. The change in gray level appears to be related to textural differences in the two bands. The inner band tends to have a compact character, while the outer band has a more open structure.

Scanning Electron Microscopy of Coating Surfaces. Secondary electron images of reacted iron filings show goethite coatings have two distinct morphologies. The most widespread coating morphology is shown in Figure 2a. At low magnification (×2500), the coating has a botryoidal appearance. Detailed examination of coatings show the grape-like mounds to be composed of sub-micrometer plates (Figure 2b). Dispersed with an apparent random distribution throughout the mounds are particulates approximately 100 nm in diameter.

Euhedral tabular crystals are also observed. These euhedral crystals occur in randomly distributed clusters (Figure 2c). Euhedral crystals occur mainly as thin plates oriented normal to the surface. Rosettes of radiating plates (Figure 2d) also occur. Many of the plates are found to be covered by delicate carpets of velvety needles (Figure 2d, upper right corner). On the surfaces of the euhedral plates in groupings that parallel blade edges are particulates similar to those observed on botryoidal surfaces (Figure 2d).

The compact character of the botryoidal goethite indicates that mineral growth occurred in a confining environment. In this study such a confining environment would be found at the points of grain contract. In contrast, the euhedral crystals indicate that unimpeded goethite growth occurred, most likely in the open interstitial areas between grains.

Secondary electron images show oxidized coatings on quartz grains are on a gross scale compact (Figure 2e) and at a fine scale comprised of delicate platelets (Figure 2f). Particulates are not observed on quartz grain coatings. However, sparsely scattered about the surface are minute authigenic columnar crystals of unknown identity.

X-ray Photoelectron Spectroscopy. *Chromium.* The $Cr(2p_{3/2})$ and $Cr(2p_{1/2})$ spectra collected from iron filing coatings are shown in Figure 3a. The former peak is centered at 577.0 eV and the latter at 586.8 eV. The magnitude of spin–orbit splitting between the full width at half maximum $2p_{1/2}$ and $2p_{3/2}$ intensities is 9.8 eV. A spin–orbit split interval of 9.8 eV is one XPS characteristic of Cr^{3+} compounds (*11*). The 2p spin–orbit split for Cr^{6+} is 9.3 eV (*11*). Further evidence for Cr^{3+} is provided by the Cr(3s) spectrum (Figure 3b). The higher energy peak centered at 79.5 eV is a 3s multiplet peak (*11*) and results from interaction of unpaired 3d electrons with core level 3s electrons of like spin during a photoelectron event (*12*). For hexavalent chromium, multiplet splitting does not occur as there is an absence of 3d electrons. The magnitudes of multiplet splittings are diagnostic for chromium valence state determination. Ikemoto et al. (*11*) report splitting magnitudes of 3.5 eV for Cr^{4+} and 3.8–3.9 eV for Cr^{3+}. The magnitude of splitting for the two 3s peaks shown in Figure 3b is 3.9 eV, also indicating the presence of trivalent chromium. The intensity ratio of the two 3s peaks is 0.6 (Table 2), which is in agreement with the theoretically predicted ratio for Cr^{3+} (*11*, *12*) and strongly indicates that spectral contributions from only trivalent chromium species occur.

The principle $Cr(2p_{3/2})$ peak (Figure 3a) has very similar binding energies and line structure to published XPS spectra for Cr_2O_3 (*11*, *13*, *14*). The doublet structure of the principle peak has been suggested to arise from multiplet interactions (*13*). Following the example of Pratt and McIntyre (*15*), the Cr(2p) spectrum is fit using calculated splitting magnitudes and intensities for the free Cr^{3+} ion (*16*). The shape of the $Cr(2p_{3/2})$ line can be fit by Gauss–Lorenz combination peak shapes whose positions and relative intensities (Table 2) agree with calculated spectra (*16*). The $Cr(2p_{1/2})$ line can similarly be fitted using predicted multiplet intensities and positions (*16*), except that a small shake-up satellite contribution (*14*) must be added at 587.9 eV (Table 2). The successful fitting of the Cr(2p) spectra suggests that chromium ions in the near-surface coating (50 Å) reside in a lattice environment similar to that in Cr_2O_3, where Cr^{3+} resides in a corundum-type

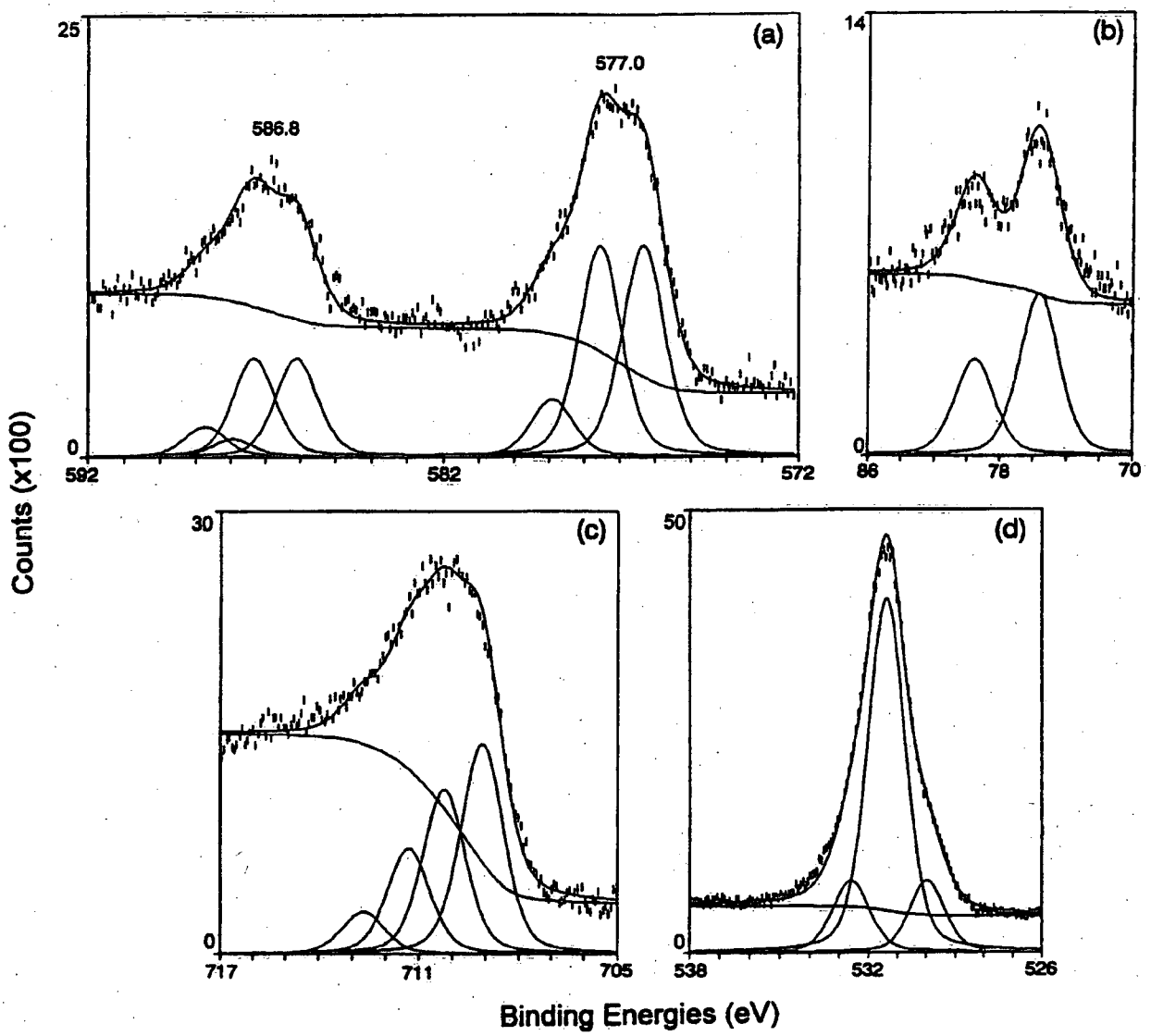

FIGURE 3. Narrow region XPS spectra collected from oxidized coatings on iron filings: (a) Cr(2p), (b) Cr(3s), (c) Fe($2p_{3/2}$), and (d) O(1s). Peak details are listed in Table 2.

structure with the cation largely ionicly bonded within an octahedral field.

Iron. The Fe($2p_{3/2}$) is centered at 710.2 eV (Figure 3c) and is fit using calculated splitting magnitudes and intensities for the free Fe^{3+}ion (*16*). Detailed discussions on the fitting of Fe(2p) spectra are presented in McIntyre and Zetaruk (*17*) and Pratt et al. (*18*). Fe($2p_{3/2}$) peak position, multiplet splitting magnitudes, and intensities (Table 2) are virtually identical to those reported by McIntyre and Zetaruk (*17*) for hematite (αFe_2O_3). Published binding energies for goethite are approximately 1.5 eV higher than those reported here (*17*). Based on these results, near-surface iron in the coatings is interpreted to be ferric and to be situated in a hematite equivalent lattice environment.

Raman spectra collected from the coatings on iron filings augment the interpretations presented above for iron and chromium. Raman spectra are characterized by two peaks with frequencies at 227 and 293 cm^{-1} and a broad substantially less intense peak near 400 cm^{-1} (see figure Supporting Information). The peaks at 227 and 293 cm^{-1} result from the detection of hematite (*19*, *20*), and the peak near 400 cm^{-1} has a shape and position diagnostic of goethite (*26*). The peaks at 227 and 293 cm^{-1} are slightly broader than those reported for hematite (*19*). However, band positions for Cr_2O_3 are known to occur near those of hematite (*20*), and the superstition of similar frequency peaks may account for the broadened appearance of peaks at 227 and 293 cm^{-1}. Furthermore, by considering that goethite species are not detected by XPS and that Raman spectroscopy is not as surface sensitive as XPS (*8*), it may be surmised that the goethite signal originates from depth, below the surface.

Oxygen. The O(1s) peak (Figure 3d) is best fit with a peak at 531.4 eV (Table 2) and is attributed to hydroxyl oxygen. The low binding energy shoulder is clearly discernible as a separate peak with a binding energy at 530.0 eV. This contribution is interpreted to originate from oxide oxygen associated with iron and chromium. These oxygen assignments are consistent with those of previous studies (*11*, *13*, *17*). To adequately fit the O(1s) spectrum, a separate peak at 532.6 eV is required. Spectral contributions near this binding energy are generally attributed to physically or chemically attached waters on oxidized iron surfaces (*21*). However, survey scans detected small amounts (<2 atomic %) of silicon. The oxygen component in SiO_2 has a binding energy of 532.9 eV (*7*). The presence of two distinct oxygen species contributing to this region of the spectrum may explain the moderate fit in the high energy toe of the spectrum using only one species (Figure 3d).

Identification that the majority of oxygen occurs as hydroxyl species appears to contradict the interpretation that

TABLE 2. XPS Narrow Region Peak Fitting Parameters, Utilized To Evaluate Spectra Collected from Iron Grains[a]

E_B	area	chemical state
Cr(3s)		
75.6	62.6	Cr(III)-O
79.5	37.4	Cr(III)-O
Cr($2p_{3/2}$)		
576.3	29.3	Cr(III)-O
577.6	29.1	Cr(III)-O
578.9	7.9	Cr(III)-O
587.9	2.4	Cr($2p_{3/2}$)-sat
Cr($2p_{1/2}$)		
586.1	13.7	Cr(III)-O
587.0	13.6	Cr(III)-O
588.7	4.0	Cr(III)-O
Fe($2p_{3/2}$)		
709.1	40.2	Fe(III)-O
710.2	31.5	Fe(III)-O
711.3	20.2	Fe(III)-O
712.7	8.1	Fe(III)-O
O(1s)		
530.0	13.7	oxide
531.4	72.1	hydroxide
532.6	14.2	water[b]

[a] Fitted peak widths (FWHM) are 1.4 eV for Cr(2p), Fe(2p), and O(1s) and 2.8 eV for Cr(3s). [b] Additional contributions from SiO_2. See text for explanation.

TABLE 3. Fe, Cr, and O Concentrations in Atomic Percent As Measured by XPS and AES Survey Scans of Iron and Quartz Grains[a]

XPS grain	Fe(3p)	Cr(3p)	O(1s)	Cr/Fe	O/(Fe + Cr)
iron	12	8	80	0.7	4.0
iron	8	13	79	1.6	3.8
Qtz	22	2	76	0.1	3.2
Qtz	11	2	87	0.2	6.7[b]

AES grain	Fe	Cr	O	Cr/Fe	O/(Fe + Cr)	EDX Cr/Fe
iron[c]	17	25	58	1.5	1.4	0.5
iron[c]	16	27	57	1.7	1.3	
iron[c]	15	27	58	1.8	1.4	
iron[c]	14	25	61	1.8	1.6	
iron[d]	16	26	58	1.6	1.4	0.2
iron[e]	13	29	58	2.2	1.4	
iron[f]	10	33	57	3.3	1.3	
Qtz	35		65		1.9	>0.1
Qtz	33		67		2.0	

[a] For comparison with the AES data, representative Cr/Fe ratios measured by EDX are also listed. [b] The increased O/(Fe + Cr) ratio is most likely due to gypsum. Ca and S were detected in the survey scan. [c] Crystallites, low particulate numbers. [d] Euhedral plate, low particulate numbers. [e] Crystallites, high particulate numbers. [f] Euhedral plate, high particulate numbers. All XPS survey scans show small amounts of Si (less than 2 atomic %).

chromium and iron are largely associated with oxide species. This apparent discrepancy can be accounted for when the pH of solution within the reaction column is considered. At the termination of the experiment, column effluent was near pH 10. The pH of the water in the column has a strong effect on the degree of protonation of water molecules coordinated with the oxide surface. In general as pH increases there is a tendency for dissociation of water molecules bound to metal oxide surfaces (*22*). The preponderance of dissociated water molecules at the oxide surface may account for the observed hydroxyl oxygen.

Concentration Trends. Atom concentrations in oxidized coatings on iron filings and quartz grains were determined using EDX, XPS, and AES. Reference standards of known concentration were not used, and all the concentration data presented were calculated using established standardless quantification procedures for each of the analytical techniques (EDX (*23*); XPS (*7*); AES (*7*)). Since reference standards were not utilized, subsequent discussions emphasize conspicuous concentration trends rather than absolute concentration fluctuations.

EDX, XPS, and AES analysis of oxide coatings on iron filings and quartz grains identify that the greatest uptake of chromium occurred on oxidized iron filing surfaces (Table 3; figure in Supporting Information). In addition, analysis by all three techniques shows that, for both grain types, the distribution of chromium is heterogeneous. For quartz surfaces, this observation is substantiated by the nondetection of chromium using AES. AES has a similar probing depth to XPS, but it samples a much smaller surface area, whereas EDX samples a similar area of the surface but its probing depth is several orders of magnitude greater than AES. It is the marked differences in the surface volumes analyzed by each technique that lead us to conclude that chromium distribution is heterogeneous in quartz grain coatings.

Due to the greater chromium content in coatings on the iron filings, microbeam analyses by EDX and AES were able to identify discernible chromium concentration trends. EDX and AES analysis of botryoidal surfaces showed both regions of low chromium content and regions of high chromium content. Inspection of the areas analyzed showed the fluctuations in chromium content varied according to the number of particulates present. In regions with high numbers of particulates, chromium content increased; whereas in regions with fewer particulates, chromium content decreased. Similar trends were observed on the euhedral plates, where particulates are particularly noticeable. These results suggest that the particulates are a chromium-rich compound, possibly Cr_2O_3. McIntyre et al. (*13*) interpret particles of similar appearance and chemistry on the surfaces of an oxidized NiCr alloy to be Cr_2O_3. Attempts to focus the electron beam of the Auger instrument to a sub-micrometer diameter and analyze a small well-defined cluster of particulates were unsuccessful. Oxygen peak intensities were observed to decrease during the period of analysis, indicating that some form of surface beam damage had occurred.

The Cr/Fe ratios determined by EDX are significantly smaller than Cr/Fe ratios measured by AES (Table 3). The difference in ratios between the two microbeam techniques can be attributed to the significantly greater probing depth of EDX relative to AES, indicating that a dilution effect occurs during EDX analysis and that surfaces are enriched in chromium relative to the bulk material. The primary significance of these observations is that in addition to chromium distribution being laterally heterogeneous, it is also heterogeneous with depth from the surface.

The O/(Fe + Cr) ratios determined by AES (Table 3) are reasonably close to the 1.5 ratio of O/Fe for hematite. This ratio is in agreement with the results and interpretations presented above for XPS and Raman spectra. AES oxygen to metal ratios obtained from quartz grain coatings, where chromium was not detected, tend to be more representative of goethite, O/Fe = 2.0 (Table 3). The AES results clearly demonstrate that surfaces exhibiting the characteristics of hematite contain chromium.

The results of this study suggest that as Cr(III) content in goethite is increased as phase transformation occurs. This phase transformation appears to be related to the breakdown of goethite into a solid species that structurally and chemically resembles hematite. Schwertmann et al. (*24*) found that goethite could structurally accommodate up to 10 mol % Cr(III). For hematite Schwertmann et al. report that Cr(III) can be fully incorporated into the αFe_2O_3 structure. Based on the work of Schwertmann et al. (*24*), it would appear that

the phase transformation takes place when goethite Cr(III) concentrations exceed 10 mol %.

The greatest chromium concentrations were found to be associated with the particulates. McIntyre et al. (*13*) attribute formation of Cr-rich particulates on NiCr surfaces to the lateral migration of Cr(III) along surfaces to points or regions of high energy (i.e., along edges or at points of intersection) where nucleation and growth would occur. We suggest the particulates observed here, formed by similar Cr migratory processes.

Acknowledgments

We thank N. S. McIntyre for providing us with access to the facilities at Surface Science Western. Financial support was provided by Natural Sciences and Engineering Research Council of Canada and the Ontario Ministry of Environment and Energy.

Supporting Information Available

Two figures showing the Raman and EDX spectra (2 pp) will appear following these pages in the microfilm edition of this volume of the journal. Photocopies of the Supporting Information from this paper or microfiche (105 × 148 mm, 24× reduction, negatives) may be obtained from Microforms Office, American Chemical Society, 1155 16th St. NW, Washington, DC 20036. Full bibliographic citation (journal, title of article, names of authors, inclusive pagination, volume number, and issue number) and prepayment, check or money order for $12.00 for photocopy ($14.00 foreign) or $12.00 for microfiche ($13.00 foreign), are required. Canadian residents should add 7% GST. Supporting Information is also available via the World Wide Web at URL http://www.chemcenter.org. Users should select Electronic Publications and then Environmental Science and Technology under Electronic Editions. Detailed instructions for using this service, along with a description of the file formats, are available at this site. To down-load the Supporting Information, enter the journal subscription number from your mailing label. For additional information on electronic access, send electronic mail to si-help@acs.org or phone (202)872-6333.

Literature Cited

(1) Kavanaugh, M. C. *Alternatives for Groundwater Cleanup*; National Academy Press: Washington, DC, 1994; p 315.
(2) Puls, R. W.; Paul, C. J.; Clark, D. A.; Vardy, J. *J. Soil Contam.* **1994**, *3*, 203–224.
(3) Powell, R. M.; Puls, R. W.; Hightower, S. K.; Sabatini, D. A. *Environ. Sci. Technol.* **1995**, *29*, 1913–1922.
(4) Mackay, D. M.; Cherry, J. A. *Environ. Sci. Technol.* **1989**, *23*, 630–636.
(5) Blowes, D. W.; Ptacek, C. J. *Subsurface Restoration Conference, 3rd International Conference on Ground Water Quality Research*, Dallas, TX, 1992; pp 214–216.
(6) Blowes, D. W.; Ptacek, C. J.; Jambor, J. L. *Environ. Sci. Technol.* Submitted for publication.
(7) Hochella, M. F., Jr. In *Spectroscopic Methods in Mineralogy and Geology*; Hawthorne, F. C., Ed.: Reviews in Mineralogy Vol. 18; Mineralogical Society of America: Washington, DC, 1988; pp 573–638.
(8) Johnston, C. T. In *Instrumental Surface Analysis of Geologic Materials*; Perry, D. L., Ed.; VCH Publishers: New York, 1990; pp 121–155.
(9) Nesbit, H. W.; Pratt, A. R. *Can. Mineral.* **1995**, *33*, 243–259.
(10) Hochella, M. F., Jr.; Turner, A. M.; Harris, D. W. *Scanning Electron. Microsc.* **1986**, *VII*, 337–349.
(11) Ikemoto, I.; Ishii, K.; Kinoshita, S.; Kuroda, H.; Franco, M. A. A.; Thomas, J. M. *J. Solid State Chem.* **1976**, *17*, 425–430.
(12) Kowalcyzyk, S. P.; Ley, L.; Mcfeely, F. R.; Shirley, D. A. *Phys. Rev. B* **1975**, 1721–1727.
(13) McIntyre, N. S.; Chan, T. C.; Chen, C. *Oxid. Met.* **1990**, *33*, 457–479.
(14) Grohman, I.; Kemmnitz, E.; Lippitz A.; Unger, W. E. S. *Surf. Interface Anal.* **1995**, *23*, 887–891.
(15) Pratt, A. R.; McIntrye, N. S. *Surf. Interface Anal.* **1996**, *24*, 529–530.
(16) Gupta, R. P.; Sen, S. K. *Phys. Rev. B* **1975**, *12*, 12–19.
(17) McIntyre, N. S.; Zetaruk, G. *Anal. Chem.* **1977**, *49*, 1521–1529.
(18) Pratt, A. R.; Muir, I. J.; Nesbitt, H. W. *Geochim. Cosmochim. Acta* **1994**, *58*, 827–841.
(19) Thibeau, R. J.; Brown, C. W.; Heidersbach, R. H. *Appl. Spectrosc.* **1978**, *32*, 532–535.
(20) Beattie I. R.; Gilson, T. R. *J. Chem. Soc. A* **1970**, 980–986.
(21) Knipe, S. W.; Mycroft, J. R.; Pratt, A. R.; Nesbitt, H. W.; Bancroft, G. M. *Geochim. Cosmochim. Acta* **1995**, *59*, 1079–1090.
(22) Schindler, P. W. In *Adsorption of Inorganics at Solid-Liquid Interfaces*; Anderson, M. A., Rubin, A. J., Eds.; Ann Arbor Science: Ann Arbor, MI, 1981; pp 1–50.
(23) Heinrich, K. F. J. *Electron Beam X-ray microanalysis*; Van Nostrand Reinhold Company: New York, 1981; p 578.
(24) Schwertmann, U.; Gasser, U.; Sticher, H. *Geochim. Cosmochim. Acta* **1989**, *53*, 1293–1297.

Received for review September 13, 1996. Revised manuscript received May 20, 1997. Accepted May 20, 1997.[⊗]

ES9607897

[⊗] Abstract published in *Advance ACS Abstracts*, July 1, 1997.

Canada Centre for Inland Waters
P.O. Box 5050
867 Lakeshore Road
Burlington, Ontario
L7R 4A6 Canada

National Hydrology Research Centre
11 Innovation Boulevard
Saskatoon, Saskatchewan
S7N 3H5 Canada

St. Lawrence Centre
105 McGill Street
Montreal, Quebec
H2Y 2E7 Canada

Place Vincent Massey
351 St. Joseph Boulevard
Gatineau, Quebec
K1A 0H3 Canada

Centre canadien des eaux intérieures
Case postale 5050
867, chemin Lakeshore
Burlington (Ontario)
L7R 4A6 Canada

Centre national de recherche en hydrologie
11, boul. Innovation
Saskatoon (Saskatchewan)
S7N 3H5 Canada

Centre Saint-Laurent
105, rue McGill
Montréal (Québec)
H2Y 2E7 Canada

Place Vincent-Massey
351 boul. St-Joseph
Gatineau (Québec)
K1A 0H3 Canada